Wang Qiyuan (Orcid ID: 0000-0003-2529-6226)
Wu Cheng (Orcid ID: 0000-0003-1288-968X)
Cao Junji (Orcid ID: 0000-0003-1000-7241)

High contribution of secondary brown carbon to aerosol light absorption in the southeastern margin of Tibetan Plateau

Qiyuan Wang[1,2*], Yongming Han[1,2], Jianhuai Ye[3], Suixin Liu[1,2], Siwatt Pongpiachan[4], Ningning Zhang[1,2], Yuemei Han[1,2], Jie Tian[1,2], Cheng Wu[5], Xin Long[1], Qian Zhang[6], Wenyan Zhang[7], Zhuzi Zhao[8], Junji Cao[1,2*]

[1]Key Laboratory of Aerosol Chemistry and Physics, State Key Laboratory of Loess and Quaternary Geology, Institute of Earth Environment, Chinese Academy of Sciences, Xi'an, 710061, China.

[2]CAS Center for Excellence in Quaternary Science and Global Change, Xi'an, 710061, China.

[3]School of Engineering and Applied Sciences, Harvard University, Cambridge, Massachusetts, 02138, USA.

[4]School of Social & Environmental Development, National Institute of Development Administration (NIDA), Bangkok, 10240, Thailand.

[5]Institute of Mass Spectrometer and Atmospheric Environment, Jinan University, Guangzhou 510632, China.

[6]School of Environmental & Municipal Engineering, Xi'an University of Architecture and Technology, Xi'an 710055, China.

[7]College of Geography, Fujian Normal University, Fuzhou, 350007, China.

[8]School of Chemical and Environmental Engineering, Jiangsu University of Technology, Changzhou, 213001, China.

This article has been accepted for publication and undergone full peer review but has not been through the copyediting, typesetting, pagination and proofreading process which may lead to differences between this version and the Version of Record. Please cite this article as doi: 10.1029/2019GL082731

*Corresponding author: Qiyuan Wang (wangqy@ieecas.cn) and Junji Cao (cao@loess.llqg.ac.cn)

Key Points:

- A statistical approach was developed to investigate secondary brown carbon (BrC) absorption over the southeastern Tibetan Plateau
- Secondary sources were the major contributors to the BrC light absorption
- Long-range transport of biomass-burning products was an important source for secondary BrC

Abstract

The optical properties of atmospheric secondary brown carbon (BrC) aerosol are poorly understood because of its chemical complexity, and this has hampered quantitative assessments of the impacts of this light-absorbing material on glaciers on the Tibetan Plateau (TP). For this study, a statistical approach was developed to investigate BrC light absorption over the southeastern margin of the TP. Secondary sources for BrC were more important for absorption than primary ones. A diurnal cycle in secondary BrC absorption was explained by the formation of light-absorbing chromophores by photochemical oxidation after sunrise followed by photobleaching of the chromophores under the more oxidizing conditions as the day progressed. Multi-method analyses showed that biomass burning in northern Burma and along the Sino-Burmese border was the most important source for the secondary BrC. The mean integrated simple forcing efficiency was 79 W g^{-1}, indicating that secondary BrC can cause substantial radiative effects.

Plain Language Summary

A statistical approach was developed to evaluate light absorption by secondary brown carbon (BrC) aerosol particles. We characterized the diurnal cycle of secondary BrC over the southeastern margin of Tibetan Plateau, identified likely pollution sources, and estimated its radiative effects. To our knowledge, this is the first time that light absorption from primary versus secondary BrC has been evaluated. This approach should be useful for further improving models and accurately evaluating the effects of BrC on glacial recession on the Tibetan Plateau.

1 Introduction

The Tibetan Plateau (TP) holds many glaciers, and the meltwater from them provides fresh water essential for a downstream population of more than 1.5 billion (Yao et al., 2012). There is growing concern that glaciers on the TP are in retreat, due in part to the influence of atmospheric black carbon (BC) and dust which are light-absorbing materials (William et al., 2010). The optical properties and radiative effects of these two substances have been well documented over the past decades (e.g., Qu et al., 2014; Zhang et al., 2015; Z. Zhao et al., 2017; Wang et al., 2018a). More recently, a group of colored organic compounds, collectively known as brown carbon (BrC), have been found to absorb sunlight, especially at short wavelengths (Andreae and Gelencsér, 2006). The radiative effects of BrC aerosols are influenced by their sources, optical properties, and chemical transformations (Yan et al.,

2018). Previous studies have shown that BrC accounts for ~20 – 40% of the total carbonaceous aerosol absorption and causes radiative effects of +0.1 to +0.6 W m^{-2} globally (Park et al., 2010; Feng et al., 2013; Wang et al., 2014; Saleh et al., 2015; Jo et al., 2016). Limited BrC studies on the TP make it difficult to evaluate effects of BrC on the radiant energy budget, and this further limits our ability to evaluate effects of BrC on glacial recession.

Atmospheric BrC either originates from primary emissions (i.e., biomass burning, coal burning, and gasoline vehicle emissions) or forms through multiphase reactions (Laskin et al., 2015). Previous studies have indicated that secondary organic aerosol from biomass burning is more absorptive for short wavelengths than the primary organic aerosol (Saleh et al., 2013), and thus, secondary BrC may be an important contributor to the global radiative forcing budget. However, direct measurements of secondary BrC light absorption are not yet feasible owing to the high chemical complexity of this material, and thus, the absorptivity of secondary BrC is not well constrained. Several studies have investigated relationships between light absorption and secondary organic carbon (SOC), and they have only described the effects of secondary BrC qualitatively (e.g., Chen et al., 2018; Li et al., 2018). Other studies have used stepwise multiple linear regression (MLR), a statistical technique, to estimate the SOC contribution to aerosol light absorption (Park et al., 2018). However, most of the compounds in SOC cause light scattering, and the use of total SOC concentrations could lead to underestimates of the light-absorbing ability of secondary BrC based on the MLR method. Additionally, some laboratory studies have explored the light-absorbing properties of secondary BrC as well as the mechanisms by which BrC forms (e.g., Nakayama et al., 2013; Song et al., 2013), but those studies have dealt with only a relatively small number of BrC species generated from typical precursors, such as toluene and α-pinene, and thus, they were not fully representative of secondary BrC in the atmosphere.

Current BrC studies on the TP have mainly focused on the sources and optical properties of total BrC or extracted water-/methanol-soluble BrC and humic-like substances (e.g., Kirillova et al., 2016; Li et al., 2016a; 2016b; Zhu et al., 2017; 2018; Wu et al., 2018). Here, a statistical approach that we call the minimum R-squared (MRS) method was developed to separate light absorption by secondary BrC versus primary BrC. The advantage of this approach is that it is simple and straightforward provided that there are suitable measurements of aerosol light absorption and BC mass concentrations. The main objectives of the study were to (1) determine the contribution of secondary sources to BrC absorption;

(2) characterize the diurnal cycle in secondary BrC absorption; (3) identify probable source regions for the high loadings of secondary BrC; and (4) evaluate the radiative effects of secondary BrC.

2 Materials and Methods

2.1 Sampling site

The southeastern margin of TP is a transitional zone between the high altitude TP (average ~4000 m above sea level, a.s.l.) and the low altitude Yunnan-Guizhou Plateau (average ~2000 m a.s.l.), and it has been recognized as one of the channels through which air pollutants from Southeast Asia are transported to the TP (S. Zhao et al., 2017). An intensive measurement campaign was conducted in this region at a site in Gaomeigu County, Yunnan Province, China (Figure S1) from 14 March to 13 May 2018. The sampling equipment was deployed on the rooftop of an office building (~10 m above ground level) of the Lijiang Astronomical Station, Chinese Academy of Sciences (100.03°E, 26.70°N; 3260 m a.s.l.). Gaomeigu County only has a resident population of more than one hundred persons, and there are no major anthropogenic sources near the sampling site.

2.2 Aerosol absorption measurement

Aerosol light absorption was measured using a multi-wavelength Aethalometer® (Model AE33, Magee Scientific, Berkeley, CA, USA) at wavelengths λ = 370, 470, 520, 590, 660, 880, and 950 nm. Ambient air was drawn into the AE33 at a flow rate of 5 L min^{-1} through a $PM_{2.5}$ cutoff, and a Nafion® dryer (MD-700-24S-3; Perma Pure, Inc., Lakewood, NJ, USA) was used to dry the particles as they entered the instrument. Detailed descriptions of the construction and operating principles of AE33 can be found in Drinovec et al. (2015). Previous studies have demonstrated that filter-based absorption measurements can suffer from nonlinear loading effects and filter matrix scattering effects (e.g., Coen et al., 2010). A two parallel spot measurement technology is embedded in AE33 to eliminate the loading effect. Meanwhile, a factor of 2.14 was used to account for the filter matrix scattering effect for the quartz filters used in this study (Drinovec et al., 2015).

2.3 Separation of secondary BrC absorption

A MRS approach for calculating the secondary BrC absorption at different wavelengths ($Abs_{BrC,sec}(\lambda)$) was developed from the widely used BC-tracer method for

calculating SOC (Srivastava et al., 2018). Aerosol light absorption is due to carbonaceous particles from both primary and secondary sources; thus, $Abs_{BrC,sec}(\lambda)$ can be calculated as:

$$Abs_{BrC,sec}(\lambda) = Abs(\lambda) - Abs_{pri}(\lambda) \quad (1)$$

where $Abs_{pri}(\lambda)$ is the light absorption at a given wavelength (e.g., λ = 370, 470, 520, 590, or 660) caused by primary light-absorbing materials from combustion and non-combustion sources. That is, $Abs_{pri}(\lambda)$ can be divided into two parts as follows:

$$Abs_{pri}(\lambda) = Abs_{pri,comb}(\lambda) + Abs_{pri,non-comb}(\lambda) \quad (2)$$

where $Abs_{pri,comb}(\lambda)$ is caused by combustion-derived primary BrC and BC, while $Abs_{pri,non-comb}(\lambda)$ is representative of non-combustion sources, which are mostly biogenic, especially plant debris and humic matter (Laskin et al., 2015). Previous studies have shown that primary biogenic aerosol mainly exists in coarse mode (Perrino and Marcovecchio, 2016), and thus we assumed a negligible effect from primary biogenic BrC in this study. As we know, BC forms during combustion processes (Petzold et al., 2013), and the combustion-derived $Abs_{pri,comb}(\lambda)$ can be estimated using a BC-tracer method:

$$Abs_{pri,comb}(\lambda) = (\frac{Abs(\lambda)}{BC})_{pri} \times [BC] \quad (3)$$

where [BC] is the mass concentration of BC, and the methods used for calculating it can be found in Text S1 of the supporting information. $(Abs(\lambda)/BC)_{pri}$ is the ratio of the primary particle's light absorption to the BC mass concentration from combustion sources. The underlying assumption of equation (3) is that the combustion-derived primary particle's absorption originates from the same sources as BC, and therefore, there is a representative ratio of primary Abs(λ)/BC for a given area. This assumption is supported by results from biomass-burning, coal-combustion, and roadside experiments (see Text S2), which show a good correlation ($R^2 > 0.98$) between primary Abs(λ) and BC mass (Figure S2). We note that $(Abs(\lambda)/BC)_{pri}$ reflects an average and effective Abs(λ)/BC ratio from mixed primary combustion sources in the atmosphere. Finally, by combined equations (1) through (3), $Abs_{BrC,sec}(\lambda)$ can be calculated by:

$$Abs_{BrC,sec}(\lambda) = Abs(\lambda) - \left(\frac{Abs(\lambda)}{BC}\right)_{pri} \times [BC] \quad (4)$$

The key step for the analyses involving equation (4) is to find a value for Abs(λ)/BC that is representative of the primary combustion sources that affected the sampling site, but finding that value is challenging because the ratio varies among sources. We used the MRS

method to exploit the presumed independence of BC and $Abs_{BrC,sec}(\lambda)$ for this purpose; that is, we assumed that the BC particles were from primary emissions while $Abs_{BrC,sec}(\lambda)$ was caused by secondary organic aerosols that mainly formed through the oxidation of organic gases (Shrivastava et al., 2017). This assumption is supported by the result of simulation of secondary BrC in biomass-burning emission (see Text S2), which showed inconsistent variations between BC mass and $Abs_{BrC,sec}(\lambda)$ formed through a Potential Aerosol Mass (PAM) flow tube reactor (Figure S3). Next, a series arbitrary values for $(Abs(\lambda)/BC)_{pri}$ (e.g., 0 – 120) was used to calculate a set of $Abs_{BrC,sec}(\lambda)$ values, and for each $(Abs(\lambda)/BC)_{pri}$ value tested, a coefficient of determination (R^2) for the relationship was derived. The series of R^2 ($Abs_{BrC,sec}(\lambda)$, BC) values was then plotted against the assumed $(Abs(\lambda)/BC)_{pri}$ values—an example of this for λ =370 nm is shown in Figure 1. The arbitrary $(Abs(\lambda)/BC)_{pri}$ value that showed the minimum R^2 for $Abs_{BrC,sec}(\lambda)$ versus BC was the target of this analysis because it best met the assumption that BC and $Abs_{BrC,sec}(\lambda)$ were independent. The MRS method avoids uncertainty caused by different arbitrary selection criterion of $(Abs(\lambda)/BC)_{pri}$, because the algorithm seeks the unique minimum point from the dataset. The bias of MRS result is < 23% when the measurement uncertainty is within 20% (Wu and Yu, 2016).

3 Results and discussion

3.1 Determination of secondary BrC absorption

The wavelength-dependence of aerosol light absorption showed a typical power law distribution in the range of 370 – 880 nm (Figure S4), and the average absorption Ångström exponent (see Text S3) was 1.6; this indicated the occurrence of BrC absorption at short wavelengths. Calculations based on the equations in Text S3 showed that the average contribution of $Abs_{BrC}(\lambda)$ to total $Abs(\lambda)$ ranged from 20% to 40% (Table S1), suggesting a substantial BrC contribution to aerosol light absorption. As the SOC fraction of organic particles from remote and sparsely populated areas is often large (Zheng et al., 2017), secondary BrC would appear to be an important contributor to $Abs_{BrC}(\lambda)$, and thus, $Abs_{BrC,sec}(\lambda)$ was further quantified using the MRS method. Considering the multiplicity of ways in which can SOC form, the measured data were divided into daytime and nighttime subsets to calculate $Abs_{BrC,sec}(\lambda)$ for those periods separately. It should be noted that when the measured $Abs(\lambda)/BC$ ratio was lower than the minimum R^2 derived $[Abs(\lambda)/BC]_{pri}$, the $Abs_{BrC,sec}(\lambda)$ would be negative, and in those cases (< 10% of data), we assumed negligible $Abs_{BrC,sec}(\lambda)$ contributions. As shown in Table 1, the average $Abs_{BrC,sec}(\lambda)$ contributed 70% of

the total Abs_{BrC} at 370 nm, 68% at 470 nm, 91% at 520 nm, 81% at 590 nm, and 77% at 660 nm with larger contributions for the daytime (73 – 98%) compared with the night (63 – 84%). These results suggest a dominant contribution from secondary sources to BrC absorption in the southeastern margin of TP, especially during the daytime. The large contributions of $Abs_{BrC,sec}(\lambda)$ at night may be attributed to the lack of photobleaching to degrade the secondary BrC chromophores. The components contributing to $Abs_{BrC,sec}(\lambda)$ were likely a diverse group of light-absorbing chromophores whose absorptivity varied with wavelength (Pretsch et al., 2009; Samburova et al., 2016). Nonetheless, similar variations in $Abs_{BrC,sec}(\lambda)$ were found for different wavelengths (Table S1), and so $Abs_{BrC,sec}(370)$ was used as a representative value to explore the characteristics of secondary BrC absorption in the following discussion.

We further used the data from biomass-burning, coal-combustion, and roadside experiments to determine the relative importance of $Abs_{BrC,sec}(\lambda)$ using the MRS method. These assessments showed that the percent contributions of $Abs_{BrC,sec}(\lambda)$ to total $Abs_{BrC}(\lambda)$ were relatively small for biomass-burning (9 – 23%), coal-combustion (9–19%), and traffic-related sources (2 – 14%) (Table 1), indicating that primary BrC absorption was more important than that from secondary BrC in fresh emissions. The small $Abs_{BrC,sec}(\lambda)$ fraction for the biomass-burning and coal-combustion tests is likely due to secondary light-absorbing chromophores that formed through gas-to-particle conversion as the combustion products mixed with the diluting air (Lipsky and Robinson, 2006). On the other hand, the $Abs_{BrC,sec}(\lambda)$ for the roadside studies may be a result of aerosol aging processes. Altogether, this analysis of source emissions data further demonstrates that the MRS method is a powerful tool for distinguishing between primary and secondary BrC light absorption.

3.2 Photochemical oxidation effects

A plot of the diurnal variation in secondary BrC absorption (Figure 2a) showed that $Abs_{BrC,sec}(370)$ decreased after midnight, reached a low value of 3.2 Mm^{-1} around 04:00 local time (LT), and then rapidly increased at a rate of 1.2 Mm^{-1} h^{-1} to a daily maximum of 6.9 Mm^{-1} around 07:00 LT. From then until 11:00, $Abs_{BrC,sec}(370)$ fluctuated at relatively high levels (6.3 – 6.6 Mm^{-1}), then it decreased sharply at a rate of 0.5 Mm^{-1} h^{-1} and reached a diurnal minimum (3.0 – 3.1 Mm^{-1}) in the afternoon around 16:00 – 17:00 LT. Finally, $Abs_{BrC,sec}(370)$ showed a small peak of 5 Mm^{-1} in the evening around 19:00 LT and later decreased once more.

The diurnal variability in $Abs_{BrC,sec}(370)$ is best explained by the combined effects of secondary particle formation, the decay of light-absorbing chromophores, and the dynamics of the planetary boundary layer (PBL). As CO is a conserved tracer of primary emissions, normalizing the $Abs_{BrC,sec}(370)$ values by the background-corrected CO mixing ratios (ΔCO) can minimize the PBL dilution effects (DeCarlo et al., 2010). Here, the background CO was defined as the lowest 1.25th percentile of the CO values measured during the entire campaign (Kondo et al., 2006) with the CO analyzer described in Text S4. As shown in Figure 2a, similar diurnal patterns were found for the normalized $Abs_{BrC,sec}(370)/\Delta CO$ ratio and $Abs_{BrC,sec}(370)$. After accounting for the effects caused by variations in the height of the PBL, the increasing trend in the $Abs_{BrC,sec}(370)/\Delta CO$ ratios from 06:00 – 11:00 LT indicates that secondary light-absorbing chromophores formed, and that was accompanied by an enhancement in $Abs_{BrC,sec}(370)$. This phenomenon can be explained by the increase in solar radiation after sunrise, which would promote photochemical reactions that led to the formation of secondary BrC.

The decreasing trend in the $Abs_{BrC,sec}(370)/\Delta CO$ ratio between 12:00 – 16:00 LT suggests that light-absorbing chromophores were bleached through oxidative processes, and that phenomenon led to decreases in $Abs_{BrC,sec}(370)$. Previous studies have shown that odd oxygen ($Ox = NO_2 + O_3$) is an indicator of air mass aging caused by photochemical reactions (Canonaco et al., 2015; Wang et al., 2017a), and a strong negative correlation between $Abs_{BrC,sec}(370)$ and Ox (see Text S4) during the daytime ($R^2 = 0.80$, Figure 2b) is another indication that photolysis and/or photo-oxidation caused photobleaching of BrC chromophores as the day progressed. This explanation is supported by recent chamber and laboratory studies, which show less absorptivity for BrC as the particles age (e.g., Sareen et al., 2013; Zhong and Jang, 2014; Zhao et al., 2015; Wong et al., 2017). Along these lines, Zhong and Jang (2014) investigated the light-absorbing properties of organic carbon from biomass burning in a large outdoor chamber under natural sunlight, and they found that light-absorption by organic carbon decreased after 8 – 9 h of sunlight exposure. Finally, the small peak in $Abs_{BrC,sec}(370)/\Delta CO$ ratios around 19:00 LT was likely related to local cooking activities because biofuels, especially wood, are used for this purpose, and the gaseous emissions from the cooking fires can lead to secondary BrC formation before sunset (~19:45 LT).

3.3 Sources of secondary BrC absorption

To identify the source regions responsible for $Abs_{BrC,sec}(370)$, a concentration-weighted trajectory (CWT) analysis was performed based on three-day air mass trajectories that were calculated backwards in time. Each hourly trajectory was calculated for arrival heights of 150 and 500 m above ground using the Hybrid Single-Particle Lagrangian Integrated Trajectory model (Draxler and Rolph, 2003), which was driven by full vertical dynamic and gridded meteorological data (Global Data Assimilation System; GDAS1, http://ready.arl.noaa.gov/HYSPLIT.php). A detailed description of the CWT procedures may be found in Wang et al. (2017b).

The CWT maps for $Abs_{BrC,sec}(370)$ (Figure 3) show that the concentration gradients were similar for the different arrival heights, and this indicates that the CWT method effectively captured the large-scale flow patterns. Large CWT values were concentrated mainly in northern Burma and along the Sino-Burmese border, indicating strong transport of secondary BrC from those areas. Further, a fire count map (Figure S5a) showed extensive biomass-burning around those areas during the sampling period, and the total number of fire counts there showed a positive correlation with $Abs_{BrC,sec}(370)$ ($R^2 = 0.47$, $p < 0.01$, Figure S5b). Combined with the CWT analysis, these results indicate that the high $Abs_{BrC,sec}(370)$ found on the southeastern margin of TP was most likely due to the long-range transport of biomass-burning-related secondary BrC from northern Burma and the Sino-Burmese border.

Moderate CWT values also were found in areas near the sampling site, suggesting that local emissions led to the formation of some secondary BrC. Pine trees and broad-leaved trees are widely distributed along the southeastern margin of TP, and therefore, the photo-oxidation of natural biogenic precursors, such as isoprene, a-pinene, and limonene (Lin et al. 2014) is a potentially important pathway for secondary BrC formation. Meanwhile, local anthropogenic emissions also may have contributed to the secondary BrC formation because even though the population in Gaomeigu is sparse, biofuels are burned by local residents. Compared with northern Burma and the Sino-Burmese border, the lower CWT values in the areas surrounding Gaomeigu indicate lesser local effects on $Abs_{BrC,sec}(370)$. Moreover, it should be noted that even though the air masses from northeast of Gaomeigu accounted for only ~4% of the total trajectories, that route may be a potential source for the high secondary BrC at times. Indeed, some of the air masses that reached the sampling site passed through areas in inland China where anthropogenic emissions are strong (Kurokawa et al., 2013).

3.4 Implications for radiative effect and atmospheric photochemistry

The potential for secondary BrC climatic impacts was evaluated through a "simple forcing efficiency" (SFE, W g^{-1}) method (Bond and Bergstrom, 2006; Chen and Bond, 2010) (see Text S5). The integrated mean SFE for secondary BrC ($SFE_{BrC,sec}$) in solar spectral range of 370 – 880 nm was 79 W g^{-1} (Figure S6a), and that accounted for 75% of total BrC SFE. Although BC was the dominant carbonaceous species in terms of a positive radiative effect (558 W g^{-1}), the fraction of secondary BrC SFE relative to BC was 14%, suggesting a non-negligible radiative effect from secondary BrC. Moreover, the proportion of $SFE_{BrC,sec}$ relative to BC increased to 23% when the air masses were influenced by biomass burning and transport was from northern Burma and the Sino-Burmese border. The uncertainty for the integrated $SFE_{BrC,sec}$ was determined quantitatively through Monte Carlo simulations. The probability distribution for $MAC_{BrC,sec}(\lambda)$ was found to be normal, and coefficients of variation (CV, defined as the standard deviation/mean) ranged from 74 – 86%. The CV for $MAC_{BrC,sec}(\lambda)$ and the normal distribution were used as input data for the Monte Carlo analysis, and 100,000 simulations were run to calculate the uncertainty. The probability distribution of $SFE_{BrC,sec}$ is shown in Figure S7. The mean, 2.5th percentile, and 97.5th percentile of integrated $SFE_{BrC,sec}$ were 79, 73, and 85 W g^{-1}, respectively, and thus, the overall uncertainty for $SFE_{BrC,sec}$ varied from -7.3% to +7.1% at the 95% confidence interval.

In addition to direct radiative effects, BrC also can influence atmospheric photochemistry indirectly by interacting with the UV wavelengths of solar radiation. For example, Jo et al. (2016) used a global 3-D chemical transport model to quantify the effects of BrC on photochemistry. Their study showed that BrC absorption could result in an 8% reduction in the annual NO_2 photolysis rate in the lower atmosphere over Asia, and that would lead to a decrease of 2 ppb in the annual surface O_3. Here we used the Tropospheric Ultraviolet and Visibility (TUV) radiation model (5.2 version, http://cprm.acom.ucar.edu/Models/TUV/Interactive_TUV) to compare the NO_2 photolysis rates for BC alone versus BC plus secondary BrC. The results (Figure S6b) indicate that the NO_2 photolysis rate would decrease by 4% due to the absorption of secondary BrC in the near-UV range (370−400 nm). This finding and the large fraction of secondary BrC we measured indicate that BrC can exert non-negligible impacts on atmospheric photochemistry over the southeastern margin of the TP, and therefore both the indirect and direct effects of BrC should be taken into account in climate assessments.

4 Conclusions

We developed a statistical approach to determine the impact of secondary BrC aerosol on light absorption over the southeastern margin of the Tibetan Plateau. The secondary BrC absorption ($Abs_{BrC,sec}(\lambda)$) accounted for 68 – 91% of the total BrC absorption, suggesting the dominant contribution from secondary sources for the southeastern margin of TP. The diurnal cycle of $Abs_{BrC,sec}(370)$ showed a rapid increase in secondary BrC formation after sunrise, whereas the light-absorbing chromophores were photobleached as a result of photo-oxidation processes in the afternoon. A strong negative correlation between odd oxygen and $Abs_{BrC,sec}(370)$ supported the idea that BrC chromophores were photobleached under more oxidizing conditions. Concentration-weighted trajectory (CWT) analyses combined with a positive relationship between $Abs_{BrC,sec}(370)$ and number of fire counts showed that biomass-burning-related secondary BrC from northern Burma and Sino-Burmese border was an important source for BrC over the southeastern margin of TP. Furthermore, photo-oxidation of biogenic precursors was recognized as a potential pathway for secondary BrC formation in the thickly forested and sparsely populated area around the sampling site. A "simple forcing efficiency" (SFE) method showed that the integrated mean SFE of secondary BrC ($SFE_{BrC,sec}$) in the solar spectral range of 370 – 880 nm was 79 W g^{-1}, and that accounted for 75% of total BrC SFE during the study. The fractional $SFE_{BrC,sec}$ relative to that of BC was 14%, and this ratio increased to 23% when the air masses were affected by biomass burning, suggesting a non-negligible radiative effect from secondary BrC. Monte Carlo simulations showed that the uncertainty for the integrated $SFE_{BrC,sec}$ varied from -7.3% to +7.1% at the 95% confidence interval. Results obtained from the Tropospheric Ultraviolet and Visibility (TUV) radiation model showed that secondary BrC absorption in the near-UV range of 370 – 400 nm may decrease the NO_2 photolysis rate by 4%, and therefore BrC evidently can influence the atmospheric photochemistry in the southeastern margin of TP.

Acknowledgments

This work was supported by the National Natural Science Foundation of China (41877391, 41661144020, and 41877404). Qiyuan Wang also acknowledged the support from the Youth Innovation Promotion Association CAS. The authors are grateful to the staff of the Lijiang Astronomical Station, Chinese Academy of Sciences, for their great assistance with field sampling. A more detailed discussion of the methodology can be found in the supporting information (Bohren and Huffman, 2008; Chow et al., 2007; Kang et al., 2007; Kondo et al., 2009; Lack and Langridge, 2013; Mao et al., 2009; Moosmüller et al., 2011; Shamjad et al., 2015; Tian et al., 2015; 2019; Wang et al., 2018b; Zhang et al., 2017). The used data are available from Fire Information for Resource Management System (https://firms.modaps.eosdis.nasa.gov) and cited sources.

References

Andreae, M. O., & Gelencsér, A. (2006). Black carbon or brown carbon? The nature of light-absorbing carbonaceous aerosols. *Atmospheric Chemistry and Physics*, 6(10), 3131–3148. https://doi.org/10.5194/acp-6-3131-2006

Bond, T. C., & Bergstrom, R. W. (2006). Light absorption by carbonaceous particles: An investigative review. *Aerosol Science and Technology*, 40(1), 27–67. https://doi.org/10.1080/02786820500421521

Bohren, C. F., & Huffman, D. R. (2008). Absorption and scattering of light by small particles. *John Wiley & Sons*.

Canonaco, F., Slowik, J. G., Baltensperger, U., & Prévôt, A. S. H. (2015). Seasonal differences in oxygenated organic aerosol composition: implications for emissions sources and factor analysis. *Atmospheric Chemistry and Physics*, 15(12), 6993–7002. https://doi.org/10.5194/acp-15-6993-2015

Chen, Y., & Bond, T. C. (2010). Light absorption by organic carbon from wood combustion. *Atmospheric Chemistry and Physics*, 10(4), 1773–1787. https://doi.org/10.5194/acp-10-1773-2010

Chen, Y., Ge, X., Chen, H., Xie, X., Chen, Y., Wang, J., et al. (2018). Seasonal light absorption properties of water-soluble brown carbon in atmospheric fine particles in Nanjing, China. *Atmospheric Environment*, 187, 230–240. https://doi.org/10.1016/j.atmosenv.2018.06.002

Chow, J. C., Watson, J. G., Chen, L. W. A., Chang, M. C. O., Robinson, N. F., Trimble, D., & Kohl, S. (2007). The IMPROVE_A temperature protocol for thermal/optical carbon analysis: Maintaining consistency with a long-term database. *Journal of the Air & Waste Management Association*, 57(9), 1014–1023. https://doi.org/10.3155/1047-3289.57.9.1014

Coen, M. C., Weingartner, E., Apituley, A., Ceburnis, D., Fierz-Schmidhauser, R., Flentje, H., et al. (2010). Minimizing light absorption measurement artifacts of the Aethalometer: evaluation of five correction algorithms, *Atmospheric Measurement Techniques*, 3(2), 457–474. https://doi.org/10.5194/amt-3-457-2010

DeCarlo, P. F., Ulbrich, I. M., Crounse, J., de Foy, B., Dunlea, E. J., Aiken, A. C.et al. (2010). Investigation of the sources and processing of organic aerosol over the Central

Mexican Plateau from aircraft measurements during MILAGRO, *Atmospheric Chemistry and Physics*, 10(12), 5257–5280. https://doi.org/10.5194/acp-10-5257-2010

Draxler, R.R., & Rolph, G.D. (2003). HYSPLIT (HYbrid Single-Particle Lagrangian Integrated Trajectory) Model access via NOAA ARL READY Website. http://www.arl.noaa.gov/ ready/hysplit4.htmlNOAA Air Resources Laboratory, *Silver Spring*, MD.

Drinovec, L., Močnik, G., Zotter, P., Prévôt, A. S. H., Ruckstuhl, C., Coz, E., et al. (2015). The "dual-spot" Aethalometer: an improved measurement of aerosol black carbon with real-time loading compensation. *Atmospheric Measurement Techniques*, 8(5), 1965–1979. https://doi.org/10.5194/amt-8-1965-2015

Feng, Y., Ramanathan, V., & Kotamarthi, V. R. (2013). Brown carbon: a significant atmospheric absorber of solar radiation?. *Atmospheric Chemistry and Physics*, 13(17), 8607–8621. https://doi.org/10.5194/acp-13-8607-2013

Jo, D. S., Park, R. J., Lee, S., Kim, S. W., & Zhang, X. (2016). A global simulation of brown carbon: implications for photochemistry and direct radiative effect. *Atmospheric Chemistry and Physics*, 16(5), 3413–3432. https://doi.org/10.5194/acp-16-3413-2016

Kang, E., Root, M. J., Toohey, D. W., & Brune, W. H. (2007). Introducing the concept of Potential Aerosol Mass (PAM). *Atmospheric Chemistry and Physics*, 7, 5727–5744. https://doi.org/10.5194/acp-7-5727-2007, 2007

Kirillova, E. N., Marinoni, A., Bonasoni, P., Vuillermoz, E., Facchini, M. C., Fuzzi, S., & Decesari, S. (2016). Light absorption properties of brown carbon in the high Himalayas. *Journal of Geophysical Research: Atmospheres*, 121(16), 9621–9639. https://doi.org/10.1002/2016JD025030

Kondo, Y., Komazaki, Y., Miyazaki, Y., Moteki, N., Takegawa, N., Kodama, D., et al. (2006). Temporal variations of elemental carbon in Tokyo. *Journal of Geophysical Research: Atmospheres*, 111, D12205. doi:10.1029/2005JD006257

Kondo, Y., Sahu, L., Kuwata, M., Miyazaki, Y., Takegawa, N., Moteki, N., et al. (2009). Stabilization of the mass absorption cross section of black carbon for filter-based absorption photometry by the use of a heated inlet. *Aerosol Science and Technology*, 43(8), 741–756. https://doi.org/10.1080/02786820902889879

Kurokawa, J., Ohara, T., Morikawa, T., Hanayama, S., Janssens-Maenhout, G., Fukui, T., et al. (2013). Emissions of air pollutants and greenhouse gases over Asian regions during 2000–2008: Regional Emission inventory in ASia (REAS) version 2, *Atmospheric Chemistry and Physics*, 13(21), 11019–11058. https://doi.org/10.5194/acp-13-11019-2013

Lack, D. A., & Langridge, J. M. (2013). On the attribution of black and brown carbon light absorption using the Ångström exponent. *Atmospheric Chemistry and Physics*, 13(20), 10535–10543. https://doi.org/10.5194/acp-13-10535-2013

Laskin, A., Laskin, J., & Nizkorodov, S. A. (2015). Chemistry of atmospheric brown carbon. *Chemical Reviews*, 115(10), 4335–4382. doi:10.1021/cr5006167

Li, C., Chen, P., Kang, S., Yan, F., Hu, Z., Qu, B., & Sillanpää, M. (2016a). Concentrations and light absorption characteristics of carbonaceous aerosol in $PM_{2.5}$ and PM_{10} of Lhasa city, the Tibetan Plateau. *Atmospheric Environment*, 127, 340–346. https://doi.org/10.1016/j.atmosenv.2015.12.059

Li, C., Yan, F., Kang, S., Chen, P., Hu, Z., Gao, S., et al. (2016b). Light absorption characteristics of carbonaceous aerosols in two remote stations of the southern fringe of the Tibetan Plateau, China. *Atmospheric Environment*, 143, 79–85. https://doi.org/10.1016/j.atmosenv.2016.08.042

Li, S., Zhu, M., Yang, W., Tang, M., Huang, X., Yu, Y., et al. (2018). Filter-based measurement of light absorption by brown carbon in $PM_{2.5}$ in a megacity in South China. *Science of The Total Environment*, 633, 1360–1369. https://doi.org/10.1016/j.scitotenv.2018.03.235

Lin, Y.-H., Budisulistiorini, S. H., Chu, K., Siejack, R. A., Zhang, H., Riva, M., et al. (2014). Light-absorbing oligomer formation in secondary organic aerosol from reactive uptake of isoprene epoxydiols. *Environmental Science & Technology*, 48(20), 12012–12021. doi:10.1021/es503142b

Lipsky, E. M., & Robinson, A. L. (2006). Effects of dilution on fine particle mass and partitioning of semivolatile organics in diesel exhaust and wood smoke. *Environmental Science & Technology*, 40(1), 155–162. doi:10.1021/es050319p

Mao, J., Ren, X., Brune, W. H., Olson, J. R., Crawford, J. H., Fried, A., et al. (2009). Airborne measurement of OH reactivity during INTEX-B, *Atmospheric Chemistry and Physics*, 9(1), 163–173. https://doi.org/10.5194/acp-9-163-2009

Moosmüller, H., Chakrabarty, R. K., Ehlers, K. M., & Arnott, W. P. (2011). Absorption Ångström coefficient, brown carbon, and aerosols: basic concepts, bulk matter, and spherical particles. *Atmospheric Chemistry and Physics*, 11(3), 1217–1225. https://doi.org/10.5194/acp-11-1217-2011

Nakayama, T., Sato, K., Matsumi, Y., Imamura, T., Yamazaki, A., & Uchiyama, A. (2013). Wavelength and NOx dependent complex refractive index of SOAs generated from the photooxidation of toluene. *Atmospheric Chemistry and Physics*, 13(2), 531–545. https://doi.org/10.5194/acp-13-531-2013

Park, R. J., Kim, M. J., Jeong, J. I., Youn, D., & Kim, S. (2010). A contribution of brown carbon aerosol to the aerosol light absorption and its radiative forcing in East Asia. *Atmospheric Environment*, 44(11), 1414–1421. https://doi.org/10.1016/j.atmosenv.2010.01.042

Park, S., Yu, G.-H., & Lee, S. (2018). Optical absorption characteristics of brown carbon aerosols during the KORUS-AQ campaign at an urban site. *Atmospheric Research*, 203, 16–27. https://doi.org/10.1016/j.atmosres.2017.12.002

Perrino, C., & Marcovecchio, F. (2016). A new method for assessing the contribution of primary biological atmospheric particles to the mass concentration of the atmospheric aerosol, *Environment International*, 87, 108–115. https://doi.org/10.1016/j.envint.2015.11.015

Petzold, A., Ogren, J. A., Fiebig, M., Laj, P., Li, S. M., Baltensperger, U., et al. (2013). Recommendations for reporting "black carbon" measurements. Atmospheric Chemistry and Physics, 13(16), 8365–8379. https://doi.org/10.5194/acp-13-8365-2013

Pretsch, E., Bühlmann, P., & Badertscher, M. (2009). Structure Determination of Organic Compounds: Tables of Spectral Data, pp. 401-420, Springer Berlin Heidelberg, Berlin, Heidelberg.

Qu, B., Ming, J., Kang, S. C., Zhang, G. S., Li, Y. W., Li, C. D., et al. (2014). The decreasing albedo of the Zhadang glacier on western Nyainqentanglha and the role of light-

absorbing impurities. *Atmospheric Chemistry and Physics*, 14(20), 11117–11128. https://doi.org/10.5194/acp-14-11117-2014

Saleh, R., Hennigan, C. J., McMeeking, G. R., Chuang, W. K., Robinson, E. S., Coe, H., et al. (2013). Absorptivity of brown carbon in fresh and photo-chemically aged biomass-burning emissions, *Atmospheric Chemistry and Physics*, 13(15), 7683–7693. https://doi.org/10.5194/acp-13-7683-2013

Saleh, R., Marks, M., Heo, J., Adams, P. J., Donahue, N. M., & A. L. Robinson (2015). Contribution of brown carbon and lensing to the direct radiative effect of carbonaceous aerosols from biomass and biofuel burning emissions. *Journal of Geophysical Research: Atmospheres*, 120(19), 10285–210296. https://doi.org/10.1002/2015JD023697

Samburova, V., Connolly, J., Gyawali, M., Yatavelli, R. L. N., Watts, A. C., Chakrabarty, R. K., Zielinska, B., Moosmüller, H., & Khlystov, A. (2016). Polycyclic aromatic hydrocarbons in biomass-burning emissions and their contribution to light absorption and aerosol toxicity. *Science of The Total Environment*, 568, 391–401. https://doi.org/10.1016/j.scitotenv.2016.06.026

Sareen, N., Moussa, S. G., & McNeill, V. F. (2013). Photochemical aging of light-absorbing secondary organic aerosol material. *The Journal of Physical Chemistry A*, 117(14), 2987–2996. doi:10.1021/jp309413j

Shamjad, P. M., Tripathi, S. N., Pathak, R., Hallquist, M., Arola, A., & Bergin, M. H. (2015). Contribution of brown carbon to direct radiative forcing over the Indo-Gangetic Plain, *Environmental Science & Technology*, 49(17), 10474–10481. doi:10.1021/acs.est.5b03368

Shrivastava, M., Cappa, C. D., Fan, J., Goldstein, A. H., Guenther, A. B., Jimenez, J. L., et al. (2017). Recent advances in understanding secondary organic aerosol: Implications for global climate forcing. *Reviews of Geophysics*, 55(2), 509–559.

Song, C., Gyawali, M., Zaveri, R. A., Shilling, J. E., & Arnott, W. P. (2013). Light absorption by secondary organic aerosol from α-pinene: Effects of oxidants, seed aerosol acidity, and relative humidity. *Journal of Geophysical Research: Atmospheres*, 118(20), 11741–11749. https://doi.org/10.1002/jgrd.50767

Srivastava, D., Favez, O., Perraudin, E., Villenave, E., & Albinet, A. (2018). Comparison of measurement-based methodologies to apportion secondary organic carbon (SOC) in $PM_{2.5}$: a review of recent studies. *Atmosphere*, 9(11), 452. https://doi.org/10.3390/atmos9110452

Tian, J., Chow, J. C., Cao, J., Han, Y., Ni, H., Chen, L.-W. A., et al. (2015). A biomass combustion chamber: Design, evaluation, and a case study of wheat straw combustion emission tests. *Aerosol and Air Quality Research*, 15(5), 2104–2114. doi:10.4209/aaqr.2015.03.0167

Tian, J., Wang, Q., Ni, H., Wang, M., Zhou, Y., Han, Y., et al. (2019). Emission characteristics of primary brown carbon absorption from biomass and coal burning: Development of an optical emission inventory for China. *Journal of Geophysical Research: Atmospheres*, doi: 10.1029/2018JD029352

Wang, Q., Huang, R., Zhao, Z., Cao, J., Ni, H., Tie, X., et al. (2017a). Effects of photochemical oxidation on the mixing state and light absorption of black carbon in the urban atmosphere of China. *Environmental Research Letters*, 12(4), 044012. https://doi.org/10.1088/1748-9326/aa64ea

Wang, Q., Zhao, Z., Tian, J., Zhu, C., Ni, H., Zhang, Y., et al. (2017b). Seasonal transport and dry deposition of black carbon aerosol in the southeastern Tibetan Plateau. *Aerosol Science and Engineering*, 1(4), 160–168. https://doi.org/10.1007/s41810-017-0016-y

Wang, Q., Cao, J., Han, Y., Tian, J., Zhu, C., Zhang, Y., et al. (2018a). Sources and physicochemical characteristics of black carbon aerosol from the southeastern Tibetan Plateau: internal mixing enhances light absorption. *Atmospheric Chemistry and Physics*, 18(7), 4639–4656. https://doi.org/10.5194/acp-18-4639-2018

Wang, Q., Cao, J., Han, Y., Tian, J., Zhang, Y., Pongpiachan, S., et al. (2018b). Enhanced light absorption due to the mixing state of black carbon in fresh biomass burning emissions. *Atmospheric Environment*, 180, 184–191. https://doi.org/10.1016/j.atmosenv.2018.02.049

Wang, X., Heald, C. L., Ridley, D. A., Schwarz, J. P., Spackman, J. R., Perring, A. E., et al. (2014). Exploiting simultaneous observational constraints on mass and absorption to estimate the global direct radiative forcing of black carbon and brown carbon.

Atmospheric Chemistry and Physics, 14(20), 10989–11010. https://doi.org/10.5194/acp-14-10989-2014

Wang, Y. Q., Zhang, X. Y., & Draxler, R. (2009). TrajStat: GIS-based software that uses various trajectory statistical analysis methods to identify potential sources from long-term air pollution measurement data, Environmental Modelling & Software, 24, 938–939. https://doi.org/10.1016/j.envsoft.2009.01.004

William, K. M. L., Maeng-Ki, K., Kyu-Myong, K., & Woo-Seop, L. (2010). Enhanced surface warming and accelerated snow melt in the Himalayas and Tibetan Plateau induced by absorbing aerosols, *Environmental Research Letters*, 5(2), 025204. doi:10.1088/1748-9326/5/2/025204

Wong, J. P. S., Nenes, A., & Weber, R. J. (2017). Changes in light absorptivity of molecular weight separated brown carbon due to photolytic aging. *Environmental Science & Technology*, 51(15), 8414–8421. doi:10.1021/acs.est.7b01739

Wu, C., & Yu, J. Z. (2016). Determination of primary combustion source organic carbon-to-elemental carbon (OC/EC) ratio using ambient OC and EC measurements: secondary OC-EC correlation minimization method. *Atmospheric Chemistry Physics*, 16(8), 5453–5465. https://doi.org/10.5194/acp-16-5453-2016

Wu, G., Wan, X., Gao, S., Fu, P., Yin, Y., Li, G., et al. (2018). Humic-like substances (HULIS) in aerosols of central Tibetan Plateau (Nam Co, 4730 m asl): Abundance, light absorption properties, and sources. *Environmental Science & Technology*, 52(13), 7203–7211. doi:10.1021/acs.est.8b01251

Yan, J., Wang, X., Gong, P., Wang, C., & Cong, Z. (2018). Review of brown carbon aerosols: Recent progress and perspectives. *Science of The Total Environment*, 634, 1475–1485. https://doi.org/10.1016/j.scitotenv.2018.04.083

Yao, T., Thompson, L. G., Mosbrugger, V., Zhang, F., Ma, Y., Luo, T., et al. (2012). Third pole environment (TPE). *Environmental Development*, 3, 52–64. https://doi.org/10.1016/j.envdev.2012.04.002

Zhang, Q., Ning, Z., Shen, Z., Li, G., Zhang, J., Lei, Y., et al. (2017). Variations of aerosol size distribution, chemical composition and optical properties from roadside to ambient environment: A case study in Hong Kong, China. *Atmospheric Environment*, 166, 234–243. https://doi.org/10.1016/j.atmosenv.2017.07.030

Zhang, R., Wang, H., Qian, Y., Rasch, P. J., Easter, R. C., Ma, P. L., et al. (2015). Quantifying sources, transport, deposition, and radiative forcing of black carbon over the Himalayas and Tibetan Plateau. *Atmospheric Chemistry Physics*, 15(11), 6205–6223. https://doi.org/10.5194/acp-15-6205-2015

Zhao, R., Lee, A. K. Y., Huang, L., Li, X., Yang, F., & Abbatt, J. P. D. (2015). Photochemical processing of aqueous atmospheric brown carbon. *Atmospheric Chemistry Physics*, 15(11), 6087–6100. https://doi.org/10.5194/acp-15-6087-2015

Zhao, S., Tie, X., Long, X., & Cao, J. (2017). Impacts of Himalayas on black carbon over the Tibetan Plateau during summer monsoon. *Science of The Total Environment*, 598, 307–318. https://doi.org/10.1016/j.scitotenv.2017.04.101

Zhao, Z., Wang, Q., Xu, B., Shen, Z., Huang, R., Zhu, C., et al. (2017). Black carbon aerosol and its radiative impact at a high-altitude remote site on the southeastern Tibet Plateau. *Journal of Geophysical Research: Atmospheres*, 122. https://doi.org/10.1002/2016JD026032

Zheng, J., Hu, M., Du, Z., Shang, D., Gong, Z., Qin, Y., et al. (2017). Influence of biomass burning from South Asia at a high-altitude mountain receptor site in China. *Atmospheric Chemistry Physics*, 17(11), 6853–6864. https://doi.org/10.5194/acp-17-6853-2017

Zhong, M., & Jang, M. (2014). Dynamic light absorption of biomass-burning organic carbon photochemically aged under natural sunlight. *Atmospheric Chemistry Physics*, 14(3), 1517–1525. https://doi.org/10.5194/acp-14-1517-2014

Zhu, C. -S., Cao, J. -J., Hu, T. -F., Shen, Z. -X., Tie, X. -X., Huang, H., et al. (2017). Spectral dependence of aerosol light absorption at an urban and a remote site over the Tibetan Plateau. *Science of The Total Environment*, 590–591, 14–21. https://doi.org/10.1016/j.scitotenv.2017.03.057

Zhu, C. -S., Cao, J. -J., Huang, R. -J., Shen, Z. -X., Wang, Q. -Y., & Zhang, N. -N. (2018). Light absorption properties of brown carbon over the southeastern Tibetan Plateau. *Science of The Total Environment*, 625, 246–251. https://doi.org/10.1016/j.scitotenv.2017.12.183

Table 1. Aerosol light absorption contributed by total brown carbon (Abs_{BrC}) and secondary brown carbon ($Abs_{BrC,sec}$) for the sampling period and for selected emission sources.

Parameter	Period	Wavelength				
		370 nm	470 nm	520 nm	590 nm	660 nm
Abs_{BrC}	Daytime	9.2[a] (36%)[b]	8.0 (39%)	4.3 (28%)	4.3 (30%)	2.8 (19%)
	Nighttime	10.6 (39%)	8.8 (41%)	4.8 (30%)	4.7 (32%)	2.7 (20%)
	All day	9.8 (38%)	8.4 (40%)	4.6 (29%)	4.5 (31%)	2.8 (20%)
$Abs_{BrC,sec}$	Daytime	7.1 (77%)[c]	5.9 (73%)	4.2 (98%)	3.7 (86%)	2.0 (73%)
	Nighttime	6.6 (63%)	5.5 (63%)	4.0 (84%)	3.5 (75%)	2.2 (82%)
	All day	6.9 (70%)	5.7 (68%)	4.1 (91%)	3.6 (81%)	2.1 (77%)
Abs_{BrC}	Biomass burning	2438 (69%)	855 (51%)	438 (37%)	255 (28%)	131 (19%)
	Coal combustion	512 (11%)	310 (9%)	232 (8%)	116 (4%)	90 (4%)
	Traffic source	11.2 (15%)	8.2 (13%)	5.2 (9%)	4.5 (9%)	3.6 (8%)
$Abs_{BrC,sec}$	Biomass burning	215 (9%)	85 (10%)	59 (14%)	49 (19%)	40 (23%)
	Coal combustion	44.8 (9%)	34.3 (11%)	27.7 (12%)	22.2 (19%)	16.8 (19%)
	Traffic source	1.2 (11%)	0.4 (5%)	0.7 (14%)	0.2 (5%)	0.1 (2%)

[a]the units for light absorption are Mm^{-1};

[b]the contribution of Abs_{BrC} to total aerosol light absorption;

[c]the contribution of $Abs_{BrC,sec}$ to Abs_{BrC}.

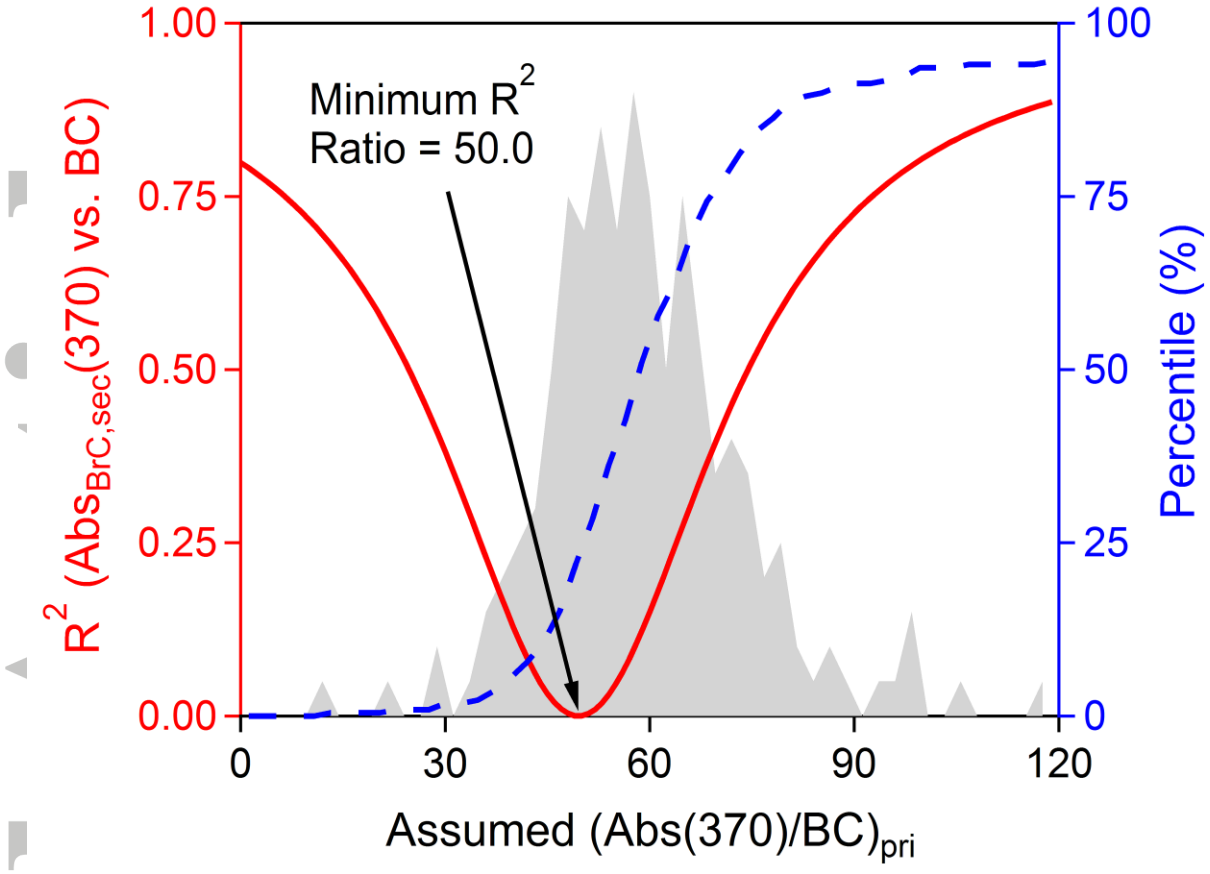

Figure 1. Coefficients of determination (R^2) for secondary brown carbon absorption at λ = 370 nm ($Abs_{BrC,sec}(370)$) versus black carbon (BC) mass concentration plotted against the primary emission ratios for light absorption and BC $(Abs(370/BC)_{pri})$. The computer program used for minimum R squared analysis may be found in https://zenodo.org/record/832396.

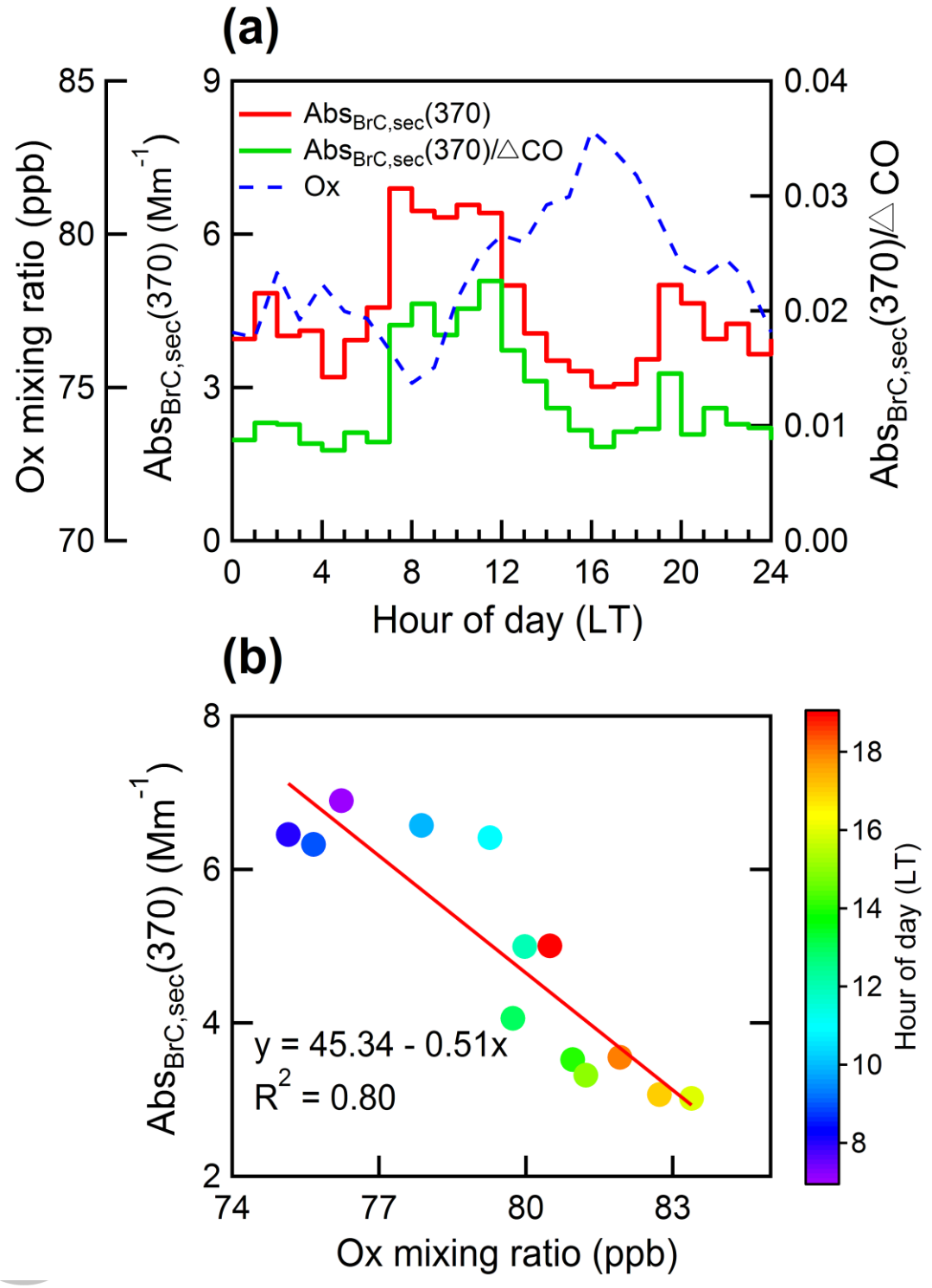

Figure 2. (a) Diurnal variations (local time, LT) of secondary brown carbon absorption at λ = 370 nm ($Abs_{BrC,sec}(370)$), $Abs_{BrC,sec}(370)$/(background-corrected CO, ΔCO), and odd oxygen (Ox = NO_2 + O_3) mixing ratios and (b) the relationship between $Abs_{BrC,sec}(370)$ and Ox during the daytime.

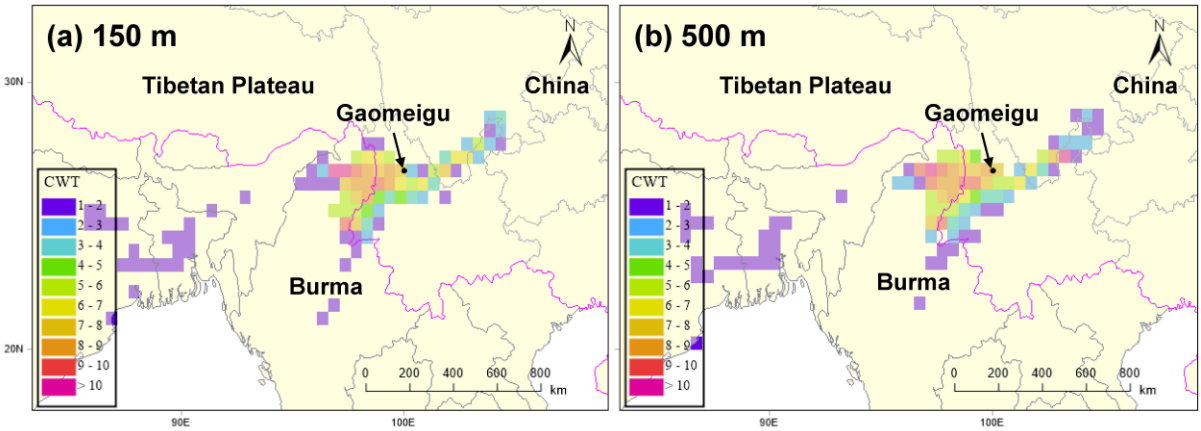

Figure 3. Maps of the concentration-weighted trajectories (CWT, Mm^{-1}) for secondary brown carbon absorption at λ = 370 nm ($Abs_{BrC,sec}(370)$) at arrival heights of (a)150 m and (b) 500 m above ground level during the campaign. The CWT analysis was conducted by the TrajStat software (Wang et al., 2009).